Supplementary Material

A Two-Stage Signal Enhancement Method Integrating Gaussian Mixture Model and Adaptive Rolling Ball Technique for Ultrasensitive Fluorescent Immunochromatographic Detection

Qian Bian [a], Chongwen Wang [c], Wenlong Bai [b], Liping Dai [b], Tao Zhang [b], Qian Wang [b], Long Zhang [a, b*], Shuai Zheng [b, d*], Shu Wang [b, *]

[a] School of Biomedical Engineering, Anhui Medical University, Hefei 230032, PR China

[b] Hefei Institute of Physical Science, Chinese Academy of Sciences, Hefei 230036, PR China

[c] Department of Clinical Laboratory Medicine, Guangdong Provincial People's Hospital (Guangdong Academy of Medical Sciences), Southern Medical University, Guangzhou 510000, PR China

[d] Wan Jiang new industry technology development center, Tongling 244000, PR China

*Corresponding author: kapposnn@163.com (Shuai Zheng); wangshu@aiofm.ac.cn (Shu Wang); zhanglong@aiofm.ac.cn (Long Zhang)

Supplementary information contents

S1. Materials section

S1.1 Preparation of Immuno-chromatographic Test Strips

The immunochromatographic test strip consisted of four components: sample pad, conjugate pad, nitrocellulose membrane, and absorbent pad, which were sequentially assembled on a plastic backing card (Jieyi Biotechnology

Co., Ltd., Shanghai, China). The nitrocellulose membranes used were UniSart CN140 and CN95 (Sartorius, Göttingen, Germany) and Whatman FF120HP membrane (Cytiva, USA). The absorbent pad was purchased from Jieyi Biotechnology Co., Ltd. (Shanghai, China).

The sample pad used in the present study was a standard general-purpose glass-fiber pad (grade GF-1, Jieyi Biotechnology Co., Ltd., Shanghai, China), which is designed for buffer-based or serum samples and is not a specialized blood-separation membrane. This general-purpose sample pad was intentionally retained throughout this study because the primary objective of this work is to develop and validate the GMM-ARB image-processing algorithm under stringent matrix interference. For applications involving direct whole-blood testing, this component can be replaced with a specialized plasma-separation pad—such as a modified asymmetric polysulfone membrane or commercially available pads (e.g., Ahlstrom CytoSep® series)—without modifying the algorithm. A comprehensive overview of available whole-blood separation strategies for POCT applications can be found in the recent review by Lee et al.

S1.2 Principle of Immuno-chromatographic Test Strip Detection

During detection, the liquid sample was applied to the sample pad and migrated toward the absorbent pad via capillary action (as shown in the figure S1). The target analyte in the sample specifically bound to the pre-immobilized quantum dot-labeled antibodies at the conjugate pad, forming antigen-antibody complexes. These complexes continued to migrate along the nitrocellulose membrane with the sample flow. Upon reaching the test line (T line), they were specifically captured by the pre-immobilized capture antibodies at this position, generating fluorescence signals under UV light excitation (365 nm). The signal intensity was positively correlated with the analyte concentration. Unbound quantum dot-labeled antibodies continued to migrate to the control line (C line), where they bound to the immobilized secondary antibodies, producing a fluorescence signal to validate the assay performance. The entire detection process was completed within approximately 10-15 minutes.

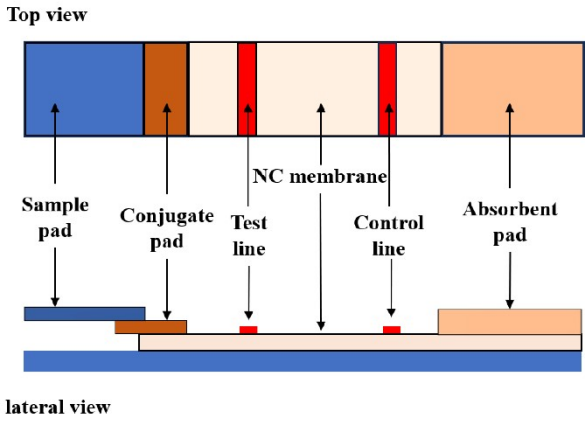

Figure S1. Schematic diagram of the fluorescent lateral flow immunochromatographic assay test strip. Top view (upper) and lateral view (lower) showing the components including sample pad, conjugate pad, nitrocellulose (NC) membrane, test line (T line), control line (C line), and absorbent pad.

S2. Hardware configuration and technical parameters of the fluorescence reader

A portable fluorescent lateral flow immunochromatographic assay (LFIA) reader was developed in-house with a modular integrated design (Figure S2a). The device measured 185 mm × 95 mm × 65 mm with a weight of approximately 500 g, and all components were enclosed in a 3D-printed plastic housing. The system was powered by a Raspberry Pi 5 development board (Raspberry Pi Foundation, Cambridge, UK) as the core processor, running

customized LFIA detection software (Version 1.0, developed in-house) based on the PyQt5 framework to enable image acquisition, signal processing, and data storage functions.

The optical excitation module consisted of a 365 nm UV-LED light source (SVC Co., Korea; output power 5 W, beam incident angle 45°) and a removable narrow-band interference filter (center wavelength 365 nm, full width at half maximum 40 nm, Thorlabs, USA), ensuring precise excitation of quantum dot fluorescent labels. The image acquisition module employed a Sony IMX179 CMOS sensor camera (Sony Corporation, Tokyo, Japan; 8-megapixel effective resolution, pixel size 1.4 μm) equipped with an autofocus lens (focal length 3.6 mm, aperture F2.0) and an exposure time set to 10 ms. The detection chamber (Figure S2b) featured a 3D-printed black cavity to shield against ambient light interference and was equipped with a contact photoelectric switch for automatic detection triggering. The device was powered by a rechargeable lithium battery (capacity 5000 mAh, operating time >8 hours), enabling truly portable operation.

The detection workflow was as follows: After launching the software and selecting the detection mode, the reacted test strip was inserted into the detection chamber, automatically triggering the detection program via the photoelectric switch. First, a visible LED illuminated, and the camera captured a visible light image for autofocusing. Subsequently, the 365 nm UV-LED, filtered through the interference filter, illuminated the test strip surface to excite the quantum dot labels, generating red fluorescence (emission peak at 620 nm). The fluorescence signal was captured by the CMOS camera with a 10 ms exposure time. The acquired fluorescence image was processed using the split function from the OpenCV library to extract the red channel, followed by two-stage signal enhancement processing using the GMM-ARB algorithm. The algorithm automatically identified the test line (T line) and control line (C line) regions, Calculate the T-line value, and output quantitative detection results. The complete detection cycle was less than 150 ms, meeting the real-time requirements for point-of-care testing (POCT).

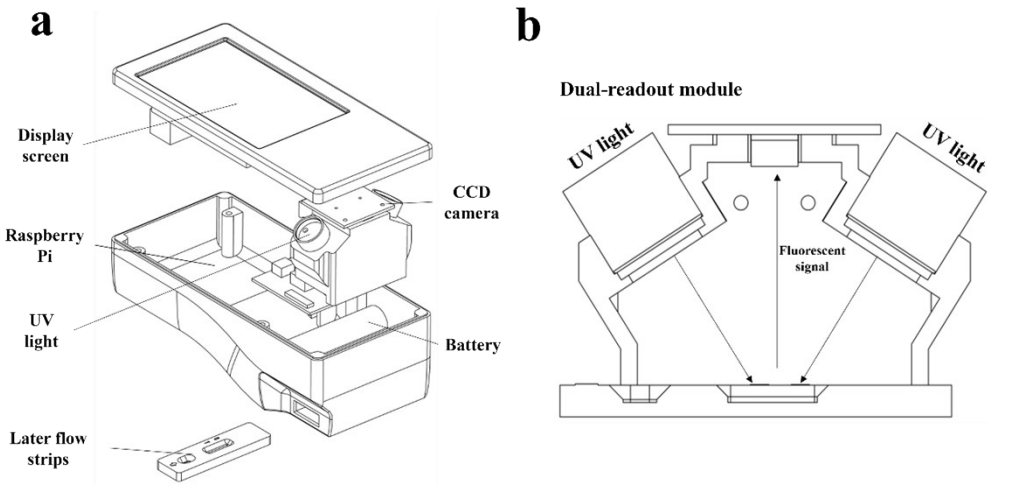

Figure S2. Schematic diagram of the portable reader for fluorescent lateral flow immunochromatographic assays. (a) Overall structure of the reader; (b) Optical detection pathway design.

S3. Preparation of experimental materials

S3.1 Synthesis of SiO_2 Microspheres

SiO_2 microspheres (~190 nm) were prepared using a modified Stöber chemical precipitation method. Briefly, 200 mL of anhydrous ethanol, 8 mL of 28% ammonia, and 12 mL of deionized water were mixed in a 250 mL flask. After stirring for 20 min at room temperature, 8 mL of TEOS was rapidly added. The mixture was continuously stirred for 6 h at room temperature. The resulting SiO_2 microspheres were collected by centrifugation (6000 rpm, 6

min), washed twice with deionized water and ethanol, and dried at 60°C in a vacuum oven.

S3.2 Synthesis of Si@DQD Nanobeads

The Si@DQD nanobeads with dual quantum dot shells were prepared through PEI-mediated electrostatic adsorption. First, 2 mg of SiO_2 microspheres were dispersed in 100 mL of deionized water by ultrasonication for 10 min. Then, 10 mL of PEI solution (0.5%, w/v) was added and ultrasonicated for 30 min to form a PEI interlayer on the SiO_2 surface. After washing twice with deionized water, 100 μL of CdSe/ZnS-MPA quantum dots (10 nM) were added to the SiO_2@PEI suspension and ultrasonicated for 45 min to form the first QD layer. The Si@QD nanobeads were collected and resuspended in 40 mL of PEI solution (0.5%, w/v), followed by ultrasonication for 30 min to form a second PEI layer. Finally, another 100 μL of quantum dots was added and ultrasonicated for 45 min to form the dual QD shell structure (Si@DQD). The resulting Si@DQD nanobeads were washed twice and stored in 10 mL of ethanol at room temperature in the dark.

S3.3 Preparation of Si@DQD Immunoprobes

The Si@DQD nanobeads were conjugated with detection antibodies through carbodiimide chemistry. Briefly, 1 mL of Si@DQD suspension (1 mg/mL) was centrifuged (4500 rpm, 6 min) and resuspended in 0.5 mL of MES buffer (10 mM, pH 5.5). Freshly prepared EDC (5 μL, 0.1 M) and NHS (10 μL, 0.1 M) were added, and the mixture was ultrasonicated for 15 min. The activated Si@DQD nanobeads were collected by centrifugation and resuspended in 0.5 mL of PBST solution (10 mM PBS, pH 7.4, containing 0.05% Tween 20). Then, 10 μg of detection antibody was added and incubated on a shaker for 2 h at room temperature. After blocking with 100 μL of 10% BSA (w/v) for 1 h, the antibody-conjugated Si@DQD immunoprobes were washed once and resuspended in 0.5 mL of storage buffer containing 10 mM PBS (pH 7.4), 0.02% NaN_3 (w/v), 1% BSA (w/v), and 0.05% Tween 20 (v/v).

S3.4 Preparation of Pathogenic Bacterial Samples

Escherichia coli, Staphylococcus aureus, and Klebsiella pneumoniae were obtained from Guangdong Provincial People's Hospital (Guangzhou, China). Bacterial strains were cultured on blood agar plates at 37°C with 5% CO_2 for 12 h. Several dozen colonies from the plate were transferred to 1 mL of PBS buffer (10 mM, pH 7.4) as the initial bacterial solution. The initial bacterial solution was diluted 10^3 to 10^5 fold in sterile water, and 0.1 mL of the diluted solution was plated on blood agar plates. To ensure the statistical accuracy and reliability of the CFU measurements (referred to as SFU in some contexts), all plating experiments were performed in triplicate. Following standard microbiological quantitative protocols, only plates containing between 30 and 300 distinct colonies after 12 h of incubation at 37°C were selected for counting. The raw counting data and calculated concentrations for the initial stocks are summarized in Table S1. The relative standard deviation (RSD) among the triplicate counts was consistently maintained below 10%, confirming the high precision of our concentration calibration baseline.

Table S1. Accuracy and reproducibility of CFU counting for the initial bacterial stock.

Pathogen	Dilution Factor	CFU Count (Plate 1)	CFU Count (Plate 2)	CFU Count (Plate 3)	Mean CFU (per 100 μL)	RSD (%)
E. coli	10^5	152	168	145	155	7.5%
S. aureus	10^5	128	134	141	134	4.8%
K. pneumoniae	10^5	110	122	115	116	5.2%

S4. Sensitivity test of fluorescence-reading equipment

To evaluate the detection sensitivity of the fluorescence reader and validate the GMM-ARB algorithm performance, quantum dot fluorescence solution assays were conducted. Red CdSe/ZnS quantum dots (excitation wavelength 365 nm, emission wavelength 625 nm, Weiyi Biotechnology Co., Ltd., Shenzhen, China) were used as fluorescent probes. Serial dilutions ranging from 10^{-11} to 10^{-4} mol L^{-1} were prepared, and 5 μL of each concentration was spotted onto nitrocellulose membrane strips and dried at room temperature before detection. Two independent measurement methods were employed for parallel comparison: (1) the GMM-ARB algorithm-based fluorescence detection platform, and (2) a multimode microplate reader (SpectraMax iD3, Molecular Devices, USA) as reference. Under 365 nm UV excitation, fluorescence signals were captured and quantified using the GMM-ARB algorithm. Four-parameter Hill equation fitting was applied: $y = A_2 + (A_1 - A_2) / [1 + (X / X_0)^p]$, where y is the fluorescence intensity, x is the quantum dot concentration, A_1 and A_2 are the maximum and minimum fluorescence signals, x_0 is the IC_{50} value, and p is the Hill coefficient. The correlation coefficient was $R^2 = 0.996$ (Figure S3). The limit of detection (LOD) calculated by the 3σ method was 1.5×10^{-10} mol L^{-1}, demonstrating good consistency with the microplate reader results (LOD = 1.8×10^{-10} mol L^{-1}), confirming the high sensitivity and reliability of the fluorescence detection system.

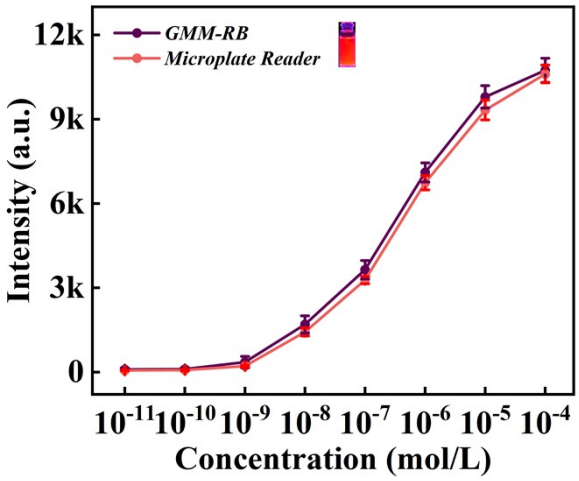

Figure S3. Sensitivity comparison between the GMM-ARB algorithm and microplate reader for quantum dot fluorescence detection. QD concentration range: 10^{-11} to 10^{-4} mol L^{-1}.

S5. Application of GMM-ARB in multiplex competitive LFIA

To evaluate the generalization capability of the proposed GMM-ARB algorithm in different assay formats, we applied the method to a multiplex competitive fluorescent lateral flow immunoassay (CFLFA) designed for the simultaneous quantitative detection of pesticide residues: imidacloprid (IMI, corresponding to the T1 line) and carbendazim (CBZ, corresponding to the T2 line). Unlike the sandwich format where signal intensity is directly proportional to target concentration, the competitive format exhibits an inverted dependency: maximum fluorescence is observed at zero concentration, and the signal progressively quenches as the target concentration increases. In practical applications, recognizing extremely weak fluorescent signals at the high-concentration end is critical to preventing premature signal truncation and broadening the dynamic range.

We processed a series of test strip images with varying concentrations using our GMM-ARB algorithm. As shown in Figure S4, traditional naked-eye observation or simple thresholding failed to distinguish the ultra-weak test line (T-line) signals from the background at high concentrations. However, the GMM-ARB algorithm effectively suppressed the non-uniform background and successfully extracted these near-threshold weak signals for both the

T1 (IMI) and T2 (CBZ) lines. The extracted absolute fluorescence intensities were perfectly fitted to a four-parameter inverse logistic curve ($R^2 > 0.99$), demonstrating that the GMM-ARB algorithm is equally reliable and highly advantageous for quantitative analysis in competitive LFIAs.

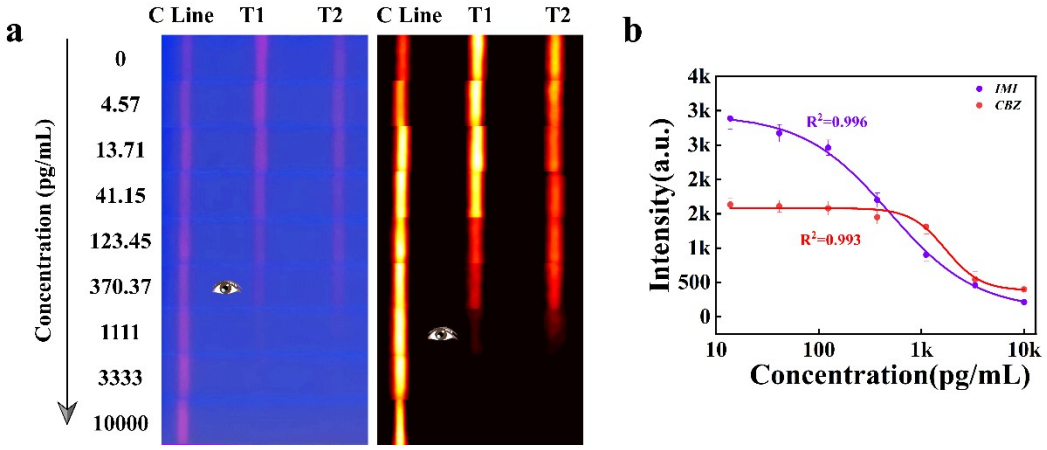

Figure S4. Application of the GMM-ARB algorithm in a multiplex competitive fluorescent lateral flow assay. (a) Original fluorescence images (left) and the corresponding GMM-ARB processed signal feature maps (right) for the simultaneous detection of imidacloprid (IMI, T1-line) and carbendazim (CBZ, T2-line). Analyte concentrations increase from top to bottom. The "eye" icons denote the naked-eye visual limit. (b) Calibration curves for IMI and CBZ based on the absolute fluorescence intensities extracted by the proposed algorithm.

S6. Stability evaluation of the hardware system

To verify the stability of the excitation light source and the image acquisition module, continuous monitoring tests were performed. As shown in Figure S5a and S5b, the working current and forward voltage of the dual UV-LEDs were continuously recorded over 120 minutes. The results exhibit negligible fluctuations, confirming the excellent reliability of the high-precision constant-current driver. Furthermore, continuous image acquisition was conducted over 600 seconds. As shown in Figure S5c and S5d, the mean grayscale values of both the T line and C line remained highly stable, and the real-time Signal-to-Noise Ratio (SNR) was consistently maintained around 32.6 dB. These results collectively demonstrate that the hardware system provides a highly uniform and stable optical field, ensuring the accuracy and repeatability of the absolute fluorescence intensity measurements.

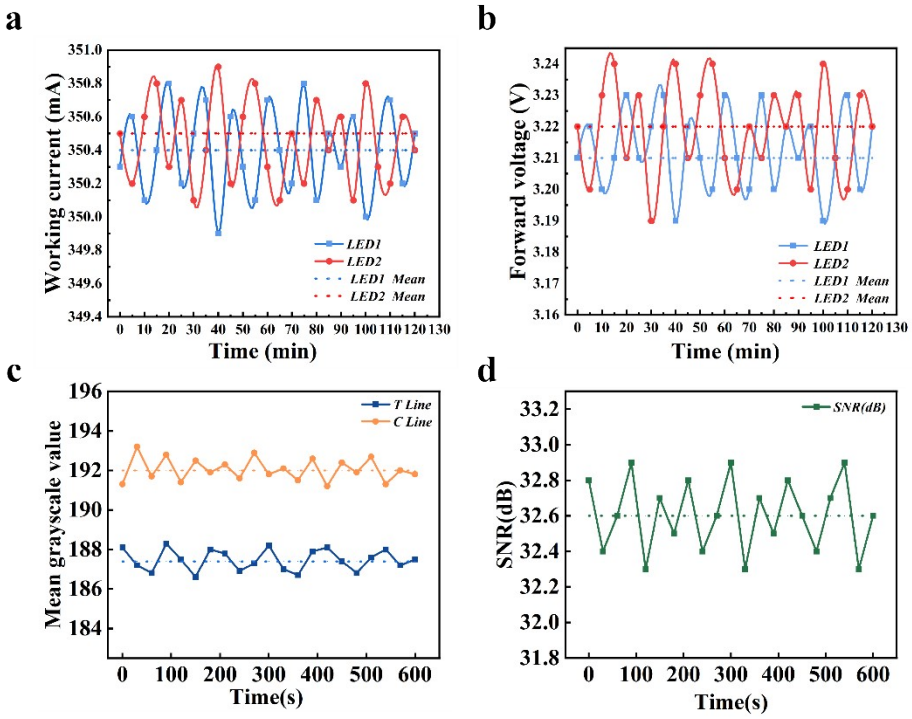

Figure S5. Hardware stability tests of the portable fluorescence reader. (a) Continuous monitoring of the working current over 120 minutes. (b) Continuous monitoring of the forward voltage over 120 minutes. (c) Stability of the mean grayscale values for the T line and C line over 600 seconds of continuous image acquisition. (d) Stability of the Signal-to-Noise Ratio (SNR) during the acquisition period.

S7. Interference evaluation using real clinical biological matrices

To evaluate the anti-interference capability of the proposed GMM-ARB algorithm against complex real-world matrix effects, an interference study was conducted referencing the CLSI EP07 guidelines. Specifically, Escherichia coli was selected as the representative pathogen and spiked into healthy human whole blood to achieve a constant final concentration of 10^3 CFU/mL. The whole blood samples were obtained from Guangdong Provincial People's Hospital, and their use was approved by the hospital's Ethics Committee (Approval No.: KY2024-677-02) with a waiver of informed consent. This specific concentration was chosen because it lies near the visual limit of detection (VLOD), representing a critical weak-signal challenge where matrix interference is most pronounced and disruptive. To systematically assess the impact of the biological matrix, the spiked whole blood was diluted with standard running buffer to create a matrix concentration gradient: 100%, 60%, 40%, 20%, 10%, and 0% (pure buffer as the baseline control). The samples were applied to the LFIA strips, and the absolute fluorescence intensities of the T-line and C-line, as well as the quantitative recovery rates, were extracted using the GMM-ARB algorithm. As shown in Figure S6, the algorithm demonstrated robust background suppression and signal extraction capabilities across a broad range of whole blood concentrations (10% to 60%), maintaining a highly stable recovery rate approaching 90-100%. This indicates that the algorithm successfully mitigates the complex optical interference and background elevation caused by blood matrices. However, at 100% whole blood concentration, both the T-line and C-line intensities dropped drastically, resulting in a recovery rate below 50%. As visually evident in the raw fluorescence images (Fig. S6a), the nitrocellulose membrane is severely darkened at 100% concentration. This signal loss is attributable to the use of a general-purpose glass-fiber sample pad in the current device, rather than to a fundamental limitation of the lateral flow format. With a non-blood-specialized sample pad, the high viscosity of intact red blood cells restricts normal capillary flow on the nitrocellulose membrane, while the dense hemoglobin strongly absorbs

both the UV excitation light and the emitted fluorescence (optical quenching), causing the membrane to appear severely darkened. As demonstrated by Ijadi Bajestani and Ahmadzadeh and comprehensively reviewed by Lee et al., specialized blood-separation membranes—such as modified asymmetric polysulfone membranes and mature commercial products (e.g., Ahlstrom CytoSep® series)—can selectively retain red blood cells while delivering cell-free plasma to the detection zone, thereby allowing direct whole-blood testing on integrated lateral flow strips. In the present study, the standard glass-fiber sample pad was intentionally retained to provide the most stringent matrix-interference challenge for evaluating the algorithm itself; integration of a specialized plasma-separation pad is a straightforward hardware upgrade that is expected to extend the operational range of the GMM-ARB-equipped reader to 100% undiluted whole blood, and this development will be pursued in our future work on fully integrated POCT diagnostics. Within the practical clinical operational range where sample dilution is standardly employed (typically yielding sample matrix concentrations below 50%), the GMM-ARB algorithm provides reliable signal recovery and quantification.

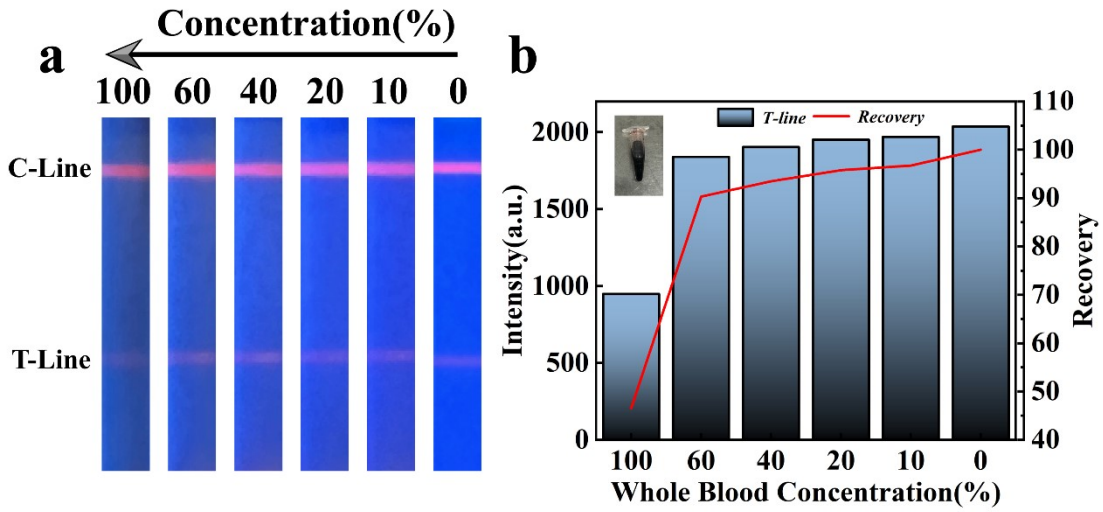

Figure S6. Anti-interference evaluation of the GMM-ARB algorithm in real healthy human whole blood matrices using *E. coli* (10^3 CFU/mL) as the target analyte. (a) Raw fluorescence images of LFIA strips tested with varying whole blood concentrations (from 100% on the left to 0% on the right). (b) Quantitative analysis showing the extracted absolute fluorescence intensities (a.u.) for the T-line (blue) alongside the analytical recovery rate (red line, %) across the corresponding whole blood concentrations.

S8. Specificity evaluation of the multiplex LFIA based on GMM-ARB

To rigorously evaluate the specificity of the proposed multiplex detection system and verify that the GMM-ARB algorithm selectively enhances genuine specific signals without amplifying non-specific cross-reactive signals, a dedicated cross-reactivity experiment was conducted. For this evaluation, a new batch of dual-target LFIA strips was independently prepared, with the K. pneumoniae capture antibody immobilized on the T1 line and the S. aureus capture antibody immobilized on the T2 line.

Four sample groups were prepared: (i) S. aureus positive only at a high concentration of 10^6 CFU/mL; (ii) K. pneumoniae positive only at 10^6 CFU/mL; (iii) double-positive sample containing both pathogens at 10^6 CFU/mL; and (iv) negative control (PBS buffer). Each sample was applied to an identical multiplex LFIA strip and analyzed by the GMM-ARB algorithm in triplicate.

As shown in Figure S7, when only S. aureus was present, a strong fluorescence signal was specifically generated at the T2 line (5659.67 ± 119.14 a.u.), while the T1 line remained at the baseline level (31.00 ± 7.51 a.u.), statistically indistinguishable from the negative control (ns, $p > 0.05$). Symmetrically, the K. pneumoniae positive sample

produced a strong signal exclusively at the T1 line (6781.33 ± 146.00 a.u.) with the T2 line remaining at baseline (29.75 ± 7.37 a.u., ns, $p > 0.05$). The double-positive sample generated distinct, simultaneous signals at both T1 (4844.67 ± 113.17 a.u.) and T2 (4839.67 ± 167.26 a.u.) lines without observable signal crosstalk, and the negative control displayed only the C line (T1: 29.00 ± 6.56 a.u.; T2: 27.67 ± 10.02 a.u.). These results confirm that the proposed GMM-ARB algorithm preserves the inherent specificity of the immunoassay and does not introduce or amplify any non-specific signals on the opposite test lines, even under high-concentration single-target challenges.

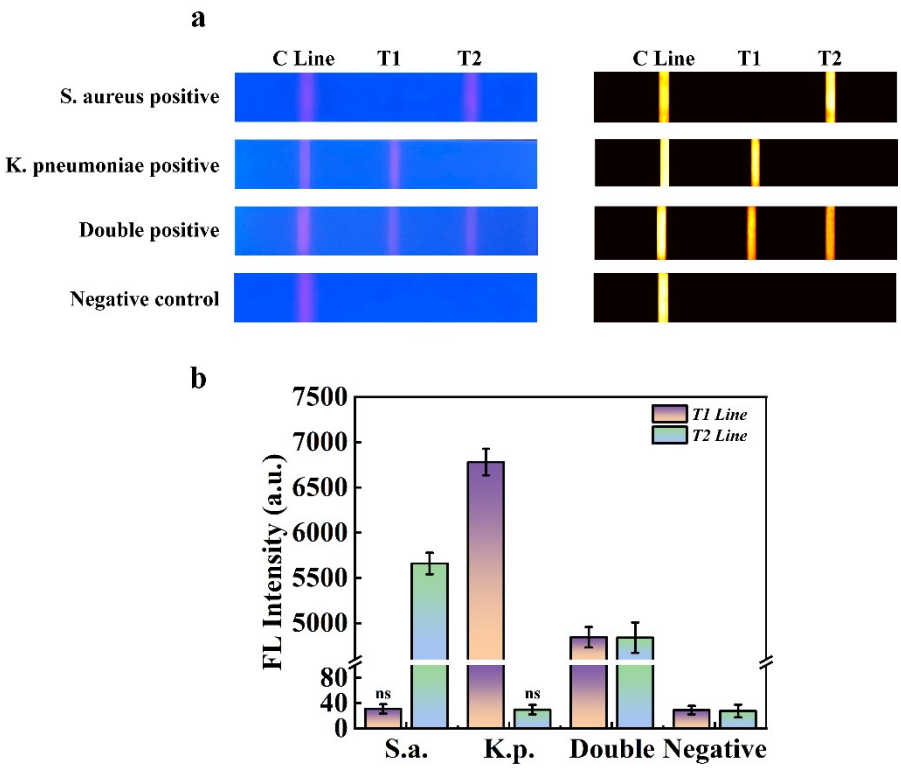

Figure S7. Specificity evaluation of the multiplex GMM-ARB-based LFIA detection. In this independent batch of test strips, the K. pneumoniae capture antibody was immobilized on the T1 line and the S. aureus capture antibody on the T2 line. (a) Raw fluorescence images (left) and the corresponding GMM-ARB-processed images (right) for four sample groups: S. aureus positive only, K. pneumoniae positive only, double positive, and negative control. (b) Quantitative fluorescence intensities of T1 and T2 lines across the four groups. "ns" indicates no statistically significant difference compared with the negative control ($p > 0.05$)